RSC Advances

PAPER

View Article Online
View Journal | View Issue

Cite this: *RSC Adv.*, 2017, **7**, 18785

Ultrasonic-induced disorder engineering on ZnO, ZrO_2, Fe_2O_3 and SnO_2 nanocrystals†

Chenyao Fan, Siqi Yu, Guodong Qian and Zhiyu Wang *

Received 27th January 2017
Accepted 23rd March 2017

DOI: 10.1039/c7ra01209h

rsc.li/rsc-advances

ZnO, ZrO_2, Fe_2O_3 and SnO_2 are all typical metal oxide semiconductors that can be used as photocatalysts for the degradation of organic pollutants in water. In this contribution, we applied the technology of ultrasonic irradiation to modify the nanocrystals (NCs) of these metal oxide semiconductors, which facilitated the hydrolysis as well as the hydroxyl injection of these NCs, resulting in the disorder engineering around their crystal lattice. The disorder modification induced band gap narrowing, the enhancement of optical absorption and inhibited recombination of photo-generated charge carriers of each metal oxide semiconductor NC, through which was eventually achieved the better performance in photocatalysis of all these materials.

Introduction

Nanostructured ZnO, ZrO_2, Fe_2O_3 and SnO_2 are all typical metal oxides showing semiconductor characters and have various applications, especially as photocatalysts. For example, ZnO, an n-type, wide band gap semiconductor, is one of the most important functional oxides for its interesting chemico-physical properties such as optical transparency, UV emission and electric conductivity, together with a good stability and low toxicity.[1,2] In particular, photocatalysis is progressively emerging for its strategic importance in the photoactivated degradation of organic pollutants.[3,4] ZnO possesses favourable optical and electrical properties of strong room temperature luminescence, high electron mobility, a wide band gap of 3.37 eV and a high exciton binding energy of 60 meV.[5] It is proposed as a suitable candidate for TiO_2 due to its similar band gap, highly efficient photocatalytic activity, lower cost and better environmental friendliness.[6]

Due to its unique characteristics such as weak acidity, basicity, redox and high thermal stability, ZrO_2 is widely used for gas sensors, ceramics, sorbents and catalysts. Concerning the latter, it is particularly employed as catalyst carrier in the selective catalytic reduction of NO by NH_3.[7] ZrO_2 is also a suitable material for photocatalyst because of its semiconducting properties,[8] low thermal conductivity, water insolubility, catalysis[9] and optical properties.[10]

Fe_2O_3 is an important n-type semiconductor oxide with an indirect band gap of 2.0–2.2 eV that allows for the absorption of substantial amounts of the incident visible solar spectrum.[11] It has attracted intensive interest due to its potential applications in magnetic recording media, gas sensors, as well as the photocatalytic degradation of organic contaminations in both water and air.[12,13]

As another typical n-type semiconductor, SnO_2 has received great attention because of its excellent stability, nontoxicity, low-cost and excellent optical electricity properties.[14] Especially, the exploitations of SnO_2 for photocatalytic water splitting and photocatalytic oxidation of organic wastes have been hot topics because of its high reduction potential and low oxidation potential.[15]

In photocatalytic process, semiconductor catalyst should harvest light with energy larger than its band gap to produce excited electrons and holes, and part of the photo-generated charges could transfer to the surface of photocatalyst before they are annihilated in the recombination and combine with adsorbed species to produce some powerful radicals, which enables a series of oxidative and reductive reactions applicable for pollutant degradation.[16] Therefore, improving the optical absorption properties and reducing electron–hole recombination are significantly expected factors for superior photocatalyst.[17]

Ultrasonic irradiation is a unique technology to fabricate nanomaterials with special physical and chemical characters. The chemical effects of ultrasonic irradiation derive primarily from the phenomenon called acoustic cavitation, which represents the ultrasonic-induced bubbles in liquid, and these bubbles go through a process including rapid formation, growth, and sudden collapse.[18,19] Such process serves to dramatically concentrate the low energy density in a sound field, generating extraordinary physicochemical conditions like

State Key Laboratory of Silicon Materials, School of Materials Science and Engineering, Zhejiang University, Hangzhou 310027, China. E-mail: wangzhiyu@zju.edu.cn

† Electronic supplementary information (ESI) available: HRTEM images, Zn 2p, Zr 3d, Fe 2p and Sn 3d XPS spectra, O 1s XPS spectra, UV-vis absorption spectra, VB XPS spectra, evaluation of dark reactions, evaluations of visible-light-driven photocatalytic activity and kinetic plots of photocatalysis, table displays k_a value of corresponding samples. See DOI: 10.1039/c7ra01209h

high local temperatures (~5200 K), high pressures (~100 MPa), very short lifetimes (<2 μs) and huge cooling and heating rates (>1 × 10^{10} °C s^{-1}).[20] So these ultrasonic-induced bubbles are named as hot spots, and the extreme environments of hot spots can effectively change the structures of some nanomaterials and confer them highly modified properties.[21–24]

In the field of nanostructured photocatalyst fabrication, ultrasonic irradiation has proven to be a facile and efficient approach to give rise to a big increase in surface area, optical absorption and photocatalytic activity of the products.[25–27] As for the metal oxide semiconductors, for example, hierarchical porous TiO_2 nanospheres[28] and ZnO porous/hollow nanospheres were fabricated under high-intensity ultrasonic irradiation.[29] Cai *et al.* synthesized ordered ZnO nanorod array film by ultrasonic spray pyrolysis[30] and further epitaxially grew SnO_2 nanowires on as-synthesized ZnO nanorod arrays, obtaining hollow cylinder ZnO/SnO_2 hierarchical nanostructures.[31] Ghosh *et al.* reported an effective sonochemistry method with an intermittent ultrasound pulse to prepare ZnO nanoflakes.[32] In another investigation, ultrasonic irradiation benefited the doping of F into TiO_2, and the F-doping benefited the formation of square-shaped morphology of TiO_2 at the same time.[33] So far, ultrasonic irradiation has been widely used to prepare metal oxide semiconductors with various nanostructures, *e.g.*, nanospheres,[28,29] 1D nanorods,[30,31] 2D nanosheets[32,33] and some nanosized composites[34,35] and hierarchical architectures.[31,36]

However, there is lack of works about the effects of ultrasonic irradiation directly acting on ready-prepared metal oxide semiconductor NCs until our previous work applied it to the modification of purchased (P25) and hydrothermally synthesized TiO_2 NCs, through which disorder phase were engineered around TiO_2 NCs, resulting in gradually narrowed band gap, enhanced optical absorption and better photocatalytic performance.[37,38] Inspired by these results, we had thought that ultrasonic irradiation might also be used to modify other metal oxide semiconductors such as ZnO, ZrO_2, Fe_2O_3 and SnO_2 NCs. To our knowledge, few references described modification of ready-prepared ZnO, ZrO_2, Fe_2O_3 and SnO_2 NCs by the direct treatment of ultrasonic irradiation before this presentation. Experimental results demonstrated the universality of disorder engineering and energy band regulation in all ultrasonic-treated metal oxide semiconductor NCs. This work proves that ultrasonic irradiation not only holds the potential in fabrication of nanostructured photocatalysts, but also a facile and universal method for disorder engineering and the resulting optical property modifications of various metal oxide semiconductor NCs.

Experimental section

Ultrasonic irradiation

The precursors of ZnO, ZrO_2, Fe_2O_3 and SnO_2 (ready-prepared NCs) were dissolved in deionized water to form pristine homogeneous suspensions with the uniform concentration of 0.1 g/100 mL respectively, then each suspension would be sent into an XH-300UL ultrasonic synthesis machine (Xianghu Science and Technology Development Limited Company, Beijing). The ultrasonic irradiation was directly acted on these NCs with a titanium alloy ultrasonic probe and a thermocouple inserting into the suspension. During the process of ultrasonic irradiation, the reaction mode was set as constant temperature at 80 °C with an output power density of 1500 W/100 mL, and the duration of ultrasonic irradiation was set as 8 h consistently. After ultrasonic irradiation, each suspension was dried at 80 °C in an oven to obtain powders of disorder engineered ZnO, ZrO_2, Fe_2O_3 and SnO_2 NCs, and we defined them as ZnO-U, ZrO_2-U, Fe_2O_3-U and SnO_2-U respectively.

X-ray diffraction (XRD)

XRD measurement was performed on all the samples using an X'Pert PRO diffractometer operating at 3 kW and a Cu K_α radiation source with continuous sweep. The scan range was 10–80° and the step size was 0.02 deg min^{-1}.

High resolution transmission electron microscopy (HRTEM)

ZnO, ZrO_2 and SnO_2 NCs and the corresponding ultrasonic-treated products were finely ground using an agate mortar and then dispersed in ethanol at an ultrasonic bath respectively. A drop of each suspension was deposited on a holey-carbon film supported on a copper 300 mesh grid. The specimens were taken micrographs by a Hitachi H-9500 HRTEM operating at 300 kV. It was noticeable that Fe_2O_3 and Fe_2O_3-U samples could not be observed by HRTEM in case of their magnetism damaging the instrument.

X-ray photoelectron spectroscopy (XPS)

All O 1s, Zn 2p, Zr 3d, Fe 2p, Sn 3d and VB XPS spectra were measured by an Escalab 250Xi spectrometer operating at an Al K_α radiation source. The binding energy was corrected for specimen charging by referencing the C 1s peak to 284.6 eV. And the accuracy of the binding energy was 0.02 eV.

Fourier transform infrared spectroscopy (FTIR)

The hydroxyls in all samples were identified by a Bruker Vector 22 Fourier infrared spectrometer (FTIR, Germany). The test samples were prepared by cold pressing a mixture of the oxides powder and potassium bromide (KBr) powder at a weight ratio of 1 : 300 to form a pellet. Transmission mode was adopted, where the scan resolution was 4 cm^{-1} and 25 scans were made and accumulated.

Diffuse reflectance UV-vis absorbance

The powders of each sample were pressed in a round glass model and a $BaSO_4$ disk was used as reference material for background measurement. All samples were measured by a Shimazu UV-4100 spectrophotometer, scanned with a speed of 300 nm min^{-1}. The intrinsic band gap value of each sample was calculated using the equation: $\alpha h\nu = A(h\nu - E_g)^p$, where α is the absorption coefficient, $h\nu$ is the photon energy, E_g is the optical band-gap, p is assumed to be 0.5 for the direct transition and A is a constant concerning the transition probability.

Brunauer–Emmett–Teller (BET) specific surface area

The surface area of each sample was obtained from N_2 adsorption/desorption isotherms by a Tristar II 3020 BET and porosity analyzer, and all samples should be preprocessed at 100 °C for 20 h to clean the surface.

Photocatalysis

The photocatalytic activity of each sample was measured by monitoring the change in concentration of acid fuchsin (AF) solution during the process of its degradation under illumination of a xenon lamp (the illumination current was 20 A and the power was 500 W). The original concentration of the AF dyestuff solution was 0.0134 g L^{-1}, and each photocatalytic system contained 150 mL of the AF solution and 0.05 g powders of metal oxide semiconductor NCs as photocatalyst. Before the photocatalysis tests, we kept each system under magnetic stirring in dark environment for at least 30 min to reach the equilibrium of surface physical adsorption, and the concentration of AF solution after this dark reaction was marked as c_0. Then the photocatalytic system was magnetic stirred for 90 min under illumination of a xenon lamp, which was used to simulate the solar irradiation, and if we settled a cut-off filter on the light source to resist the light with wavelength shorter than 400 nm, the visible-light irradiation could be selected. For each photocatalytic system, we took sample from degradative AF solution for every 5 or 10 min and used centrifugation to get rid of the photocatalyst powders inside. The concentration of extractive AF solution was marked as c, so the value of c/c_0 represented the degree of degradation of AF solution. Based on Lambert–Beer's law, the concentration ratio equals to the corresponding UV-vis absorbance ratio, which could be measured by a Shimadzu UV-4100 spectrophotometer (scanned from 175 nm to 800 nm; scanning speed was 300 nm min^{-1}). The change of concentration ratio against illumination time figured out the concentration decrease rate of AF solution, which evaluated the photocatalytic activity of the corresponding metal oxide semiconductor sample.

Results and discussion

In order to promote the universality of this research, we purchased ready-prepared ZnO, ZrO_2, Fe_2O_3 and SnO_2 NCs as precursors, which made sure that no particular synthesis conditions or pretreatments could affect the modification results. For each kind of metal oxide semiconductor NCs, we compare the differences in structures and properties before and after ultrasonic irradiation. As one of the main features, there is the obvious colour change for the ultrasonic-treated metal oxide semiconductor NCs. White NCs of ZnO, ZrO_2 and SnO_2 turned to gray while the rusty red Fe_2O_3 NCs became reddish black (Fig. 1). The XRD patterns (Fig. 2) demonstrate almost identical peak locations between precursor and ultrasonic-treated product of each metal oxide semiconductor NCs, indicating that phase composition remained the same during the process of ultrasonic irradiation. Meanwhile, diffraction peaks have decreased height and broadened linewidth with different

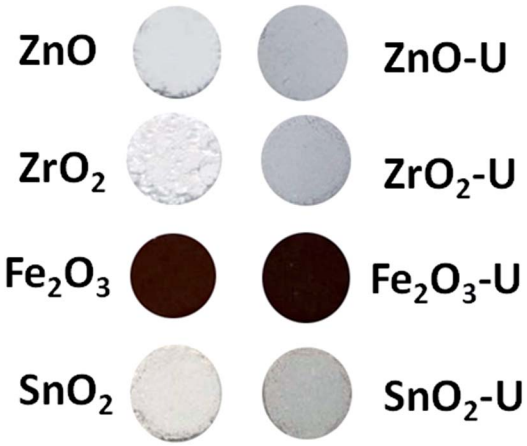

Fig. 1 Photos comparing the colour in appearance of ZnO, ZrO_2, Fe_2O_3, SnO_2 NCs and the corresponding ultrasonic-treated products.

degrees, which means the reduced crystallinity in this process. Specific calculation results of average NC size on dominant facet through Scherrer equation (Table 1) demonstrate the shrink of NCs to some degree in each ultrasonic-treated product. Further investigation by HRTEM images (Fig. S1†) show the totally crystalline precursors and disorder phase around crystal lattice (the boundaries are marked by white lines in Fig. S1†) in ultrasonic-treated products. The disorder engineering means the significant broken of structure,[17] which could only induced by the strong ultrasonic irradiation in our experimental conditions, also well explains the reduced crystallinity and NC shrinking that drawn from XRD patterns.

The chemical composition of each sample are investigated by XPS, which displays no significant changes in Zn 2p, Zr 3d, Fe 2p and Sn 3d XPS spectra (Fig. S2†) through ultrasonic irradiation, indicating the constant valence of each metal element and eliminating the possibility of self-doping by reduced metal ions in this process. High-intensity ultrasonic irradiation could largely promote the mass transfer between the liquid–solid interfaces. Cavitations and shock waves generated by ultrasound facilitate the decomposition of chemical bonds and the exchange of species.[16] So the reaction of hydrolysis are certainly more active under this condition. In such case, we use O 1s XPS to demonstrate the situation of hydrolysis in ZnO, ZrO_2, Fe_2O_3 and SnO_2 NCs through ultrasonic irradiation. The O 1s XPS spectra of all the samples (Fig. S3†) can be divided into two peaks that attributed to two kinds of binding oxygen, *i.e.*, the main peaks locating between 528.1 eV and 531.1 eV that attributed to bridge oxygen in crystalline matrix (X–O–X) and the additional peaks locating between 530.9 eV and 532 eV that attributed to oxygen in hydroxyls (X–OH).[39] The quantitative determination based on peak areas works out the ratio of X–OH/X–O of each sample (X represents for Zn, Zr, Fe or Sn), which indicates the significant growing amount of hydroxyls in all the ultrasonic-treated products (Table 1).

Apparently, the ultrasonic-induced hydroxylation results from the facilitative hydrolysis reaction. The extraordinary physicochemical conditions under ultrasonic irradiation excites

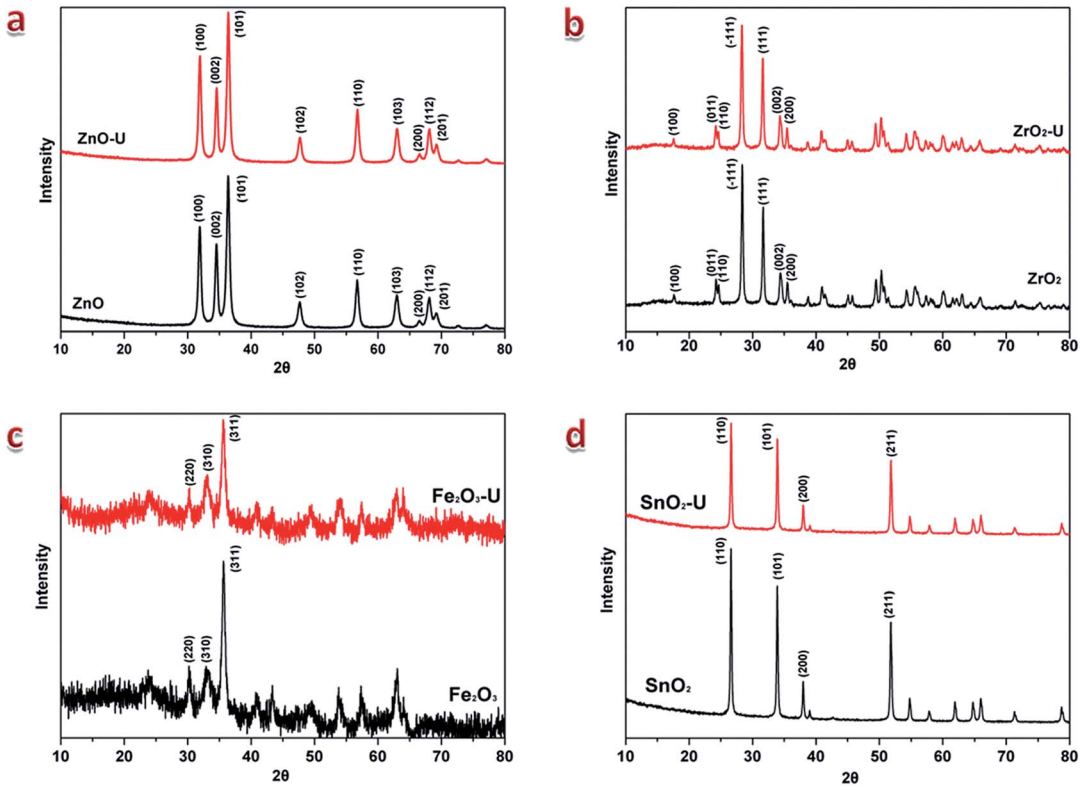

Fig. 2 XRD patterns of ZnO, ZrO_2, Fe_2O_3, SnO_2 NCs and the corresponding ultrasonic-treated products.

Table 1 Average NC sizes, hydroxylation degrees (X–OH/X–O ratio) and BET specific surface areas (S_{BET}) of ZnO, ZrO_2, Fe_2O_3, SnO_2 NCs and the corresponding ultrasonic-treated products

Sample	ZnO	ZnO-U	ZrO_2	ZrO_2-U	Fe_2O_3	Fe_2O_3-U	SnO_2	SnO_2-U
Crystal size/nm	17.09	16.15	28.18	27.09	15.78	14.68	33.64	32.95
X–OH/X–O	0.66	0.93	0.68	0.98	0.57	0.96	0.44	0.98
$S_{BET}/m^2\ g^{-1}$	25.01	37.39	17.32	28.77	25.52	38.40	15.95	26.21

high concentration of active radicals of $OH^{\bullet}$ and $H^{\bullet}$ in water, which attacks the surface of metal oxide semiconductor NCs, causing the chemical bond decomposition of crystalline matrix and following by restructuring with hydroxyls injection. The whole reaction could be summarized by equation: $XO_n + mH_2O \rightarrow XO_{n-m}(OH)_{2m}$, where XO_n represents for ZnO, ZrO_2, Fe_2O_3 and SnO_2 respectively. The broken structure caused by ultrasonic-induced hydroxylation results in the disorder engineering on NCs as displayed in HRTEM images and XRD patterns. The hydroxylation in products of $XO_{n-m}(OH)_{2m}$ can be used to determine the degree of disorder, more hydroxyls injection means more restructuring. The ultrasonic-induced hydroxylation can further be confirmed by FTIR spectra (Fig. 3). It shows the peaks at ~3460 cm^{-1} and ~1630 cm^{-1} that attributed to the stretching and bending vibrational bands of hydroxyls[40] in all samples. The stronger intensity of hydroxyl peaks in ultrasonic-treated products indicates the ultrasonic-induced hydroxylation, and a little bit blue-shift of the hydroxyl stretching vibrational band at ~3460 cm^{-1} suggests the formation of surface defects after ultrasonic irradiation. These experimental results prove the universality of the mechanism of disorder engineering on ZnO, ZrO_2, Fe_2O_3 and SnO_2 NCs by the effects of ultrasonic-induced hydroxylation.

The marked colour changes of ultrasonic-treated products suggest the differences in optical absorption. UV-vis spectral absorbance of all the samples (Fig. S4†) demonstrate the enhancement of optical absorption through the whole regions with wavelength larger than corresponding absorption edges of each metal oxide semiconductor NCs after ultrasonic irradiation. The wavelength-extended and intensity-enhanced absorption covers most of the visible-light region and matches the deeper colours of ultrasonic-treated products (Fig. 1). The energy band structure is the essential factor that determines various properties, including colour, optical absorption and photocatalytic activity. From the calculation and fitting that based on absorption edges (see details in Experimental section), we find out the narrower intrinsic band gaps for all ultrasonic-treated metal oxide semiconductor NCs than the corresponding precursors (marked by black arrows in Fig. 4). Moreover, VB XPS spectra (Fig. S5†) clearly show the valance band tails induced by

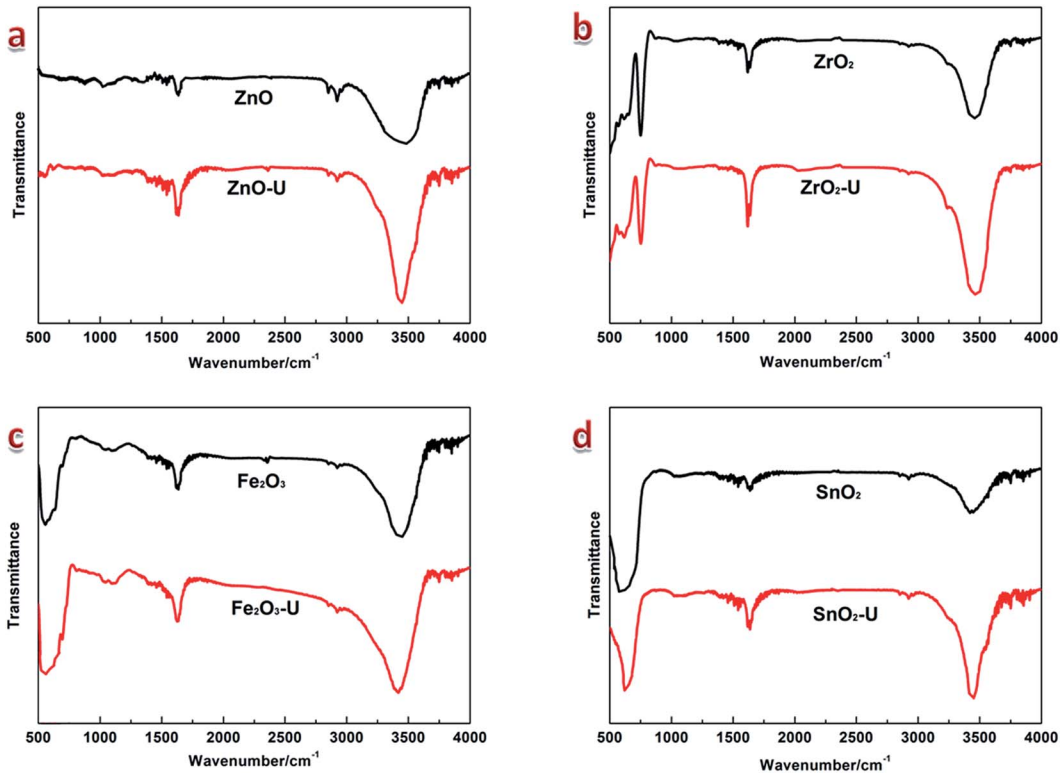

Fig. 3 FTIR spectra of ZnO, ZrO_2, Fe_2O_3, SnO_2 NCs and the corresponding ultrasonic-treated products.

the blue-shifted valance band maximum (VBM) towards Fermi level in ultrasonic-treated products, causing the further narrowing of band gaps (marked by blue arrows in Fig. 4), which is the direct reason for enhanced optical absorption. The schematic illustrations of the density of states (DOS) intuitively display the band tails and narrowed band gaps of ultrasonic-treated metal oxide semiconductor NCs (Fig. 4). The disorder engineering is the critical factor inducing band tails because the distortion of crystal lattice changes the electronic structures.[41] The VBM of metal oxide semiconductor NCs is mainly derived from O 2p orbitals while the conduction band minimum (CBM) is mainly determined by electronic structure of metal atoms.[42] The distortion of crystal lattice will induce blue-shift of VBM as well as red-shift of CBM, which both result in band tail. But considering the lower energy barrier to deform O sublattice,[43] valance band tail induced by blue-shifted VBM plays the dominant role in band gap narrowing. The band gap narrowing in ultrasonic-treated metal oxide semiconductor NCs reduces the difficulty of electron transition and improves the utilization of light energy, which not only is the direct reason for the enhancement of optical absorption but also indicates the potential of higher photocatalytic activity.

The photocatalytic activity of each sample was evaluated by its catalytic degradation rate of acid fuchsin (AF) solution under illumination. BET specific surface area tests demonstrate the growing surface area through ultrasonic irradiation of all these metal oxide semiconductor NCs (Table 1). Larger surface area, on one hand, attracts more reactive radicals and provides more reactive sites on photocatalyst surface, which helps to achieve better photocatalytic performance. On other hand, the self-sensitive effect will also be promoted for the higher physical adsorption induced by larger surface area. In order to obtain the accurate photocatalytic activity of each sample, pretreatment of dark reaction (Fig. S6†) is needed, and then the photocatalysis tests under illumination can be carried on (see details in Experimental section). The test results of solar-driven photocatalytic activity in Fig. 5 exhibit the higher degradation rate for all these ultrasonic-treated products than the corresponding precursors. The simulation results of kinetic constants (k_a) based on Langmuir–Hinshelwood model: $\ln(c_0/c) = k_a t$ are displayed in Fig. 6 and Table S1,† which indicates that the solar-driven photocatalytic activity for AF degradation are increased for ~27% (ZnO), ~43% (ZrO_2), ~46% (Fe_2O_3) and ~74% (SnO_2) respectively through ultrasonic irradiation. Compared to the changes in hydroxylation, as well as the degree of disorder (Table 1), it can be discovered that more disorder engineering brings larger enhancement in solar-driven photocatalytic activity. This is because of the localized band tails and surface defects that induced by lattice distortion in ultrasonic-treated metal oxide semiconductor NCs acting as effective trap sites for photo-generated electrons and holes, which restrain the recombination of charge carriers.[43] Moreover, larger surface area induced by disorder engineering afford more adsorbates, once the photo-generated electrons and holes migrate to NC surface, they could immediately take part in reactions like dissolved oxygen reduction and organic molecules oxidization respectively, which suppresses their recombination as well. Besides, the band gap narrowing enlarges the scale of photo-

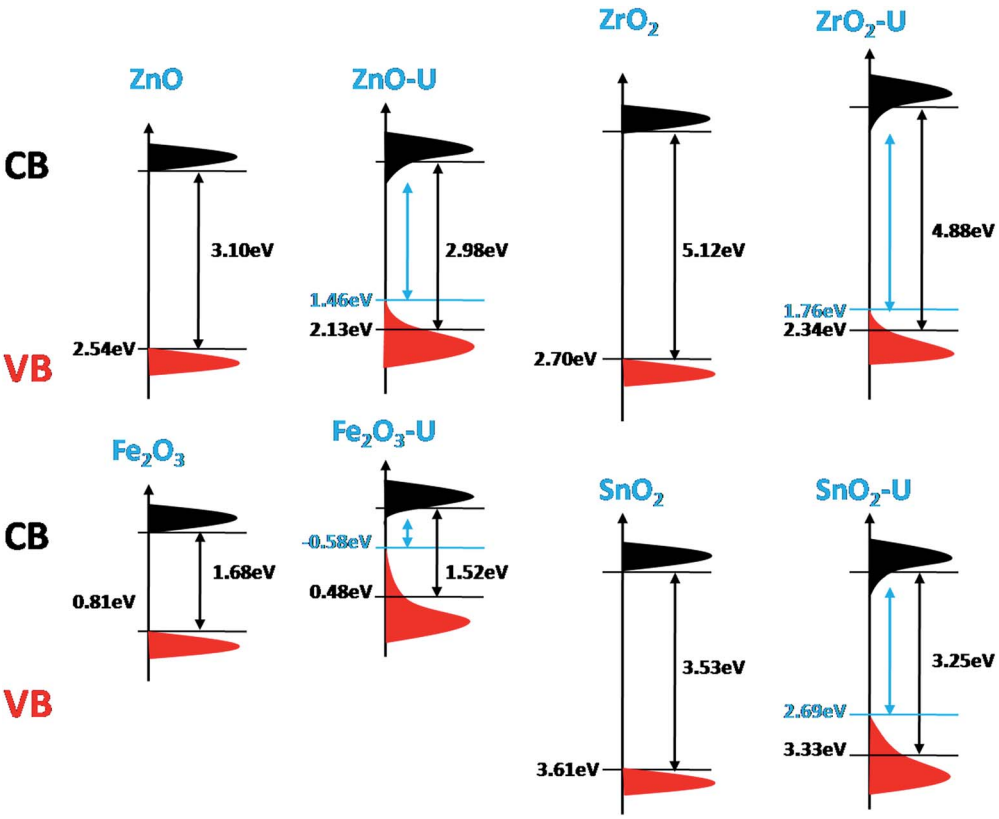

Fig. 4 Schematic illustrations of DOS of ZnO, ZrO_2, Fe_2O_3, SnO_2 NCs and the corresponding ultrasonic-treated products.

response wavelength and the intensity of absorbance, which gives rise to more light energy utilization in all ultrasonic-treated products. Considering the proper VB location and band gap value, electron transition in ZnO and Fe_2O_3 NCs can be excited by visible-light illumination. In this situation, photo-generated charge carriers are insufficient since the excitation

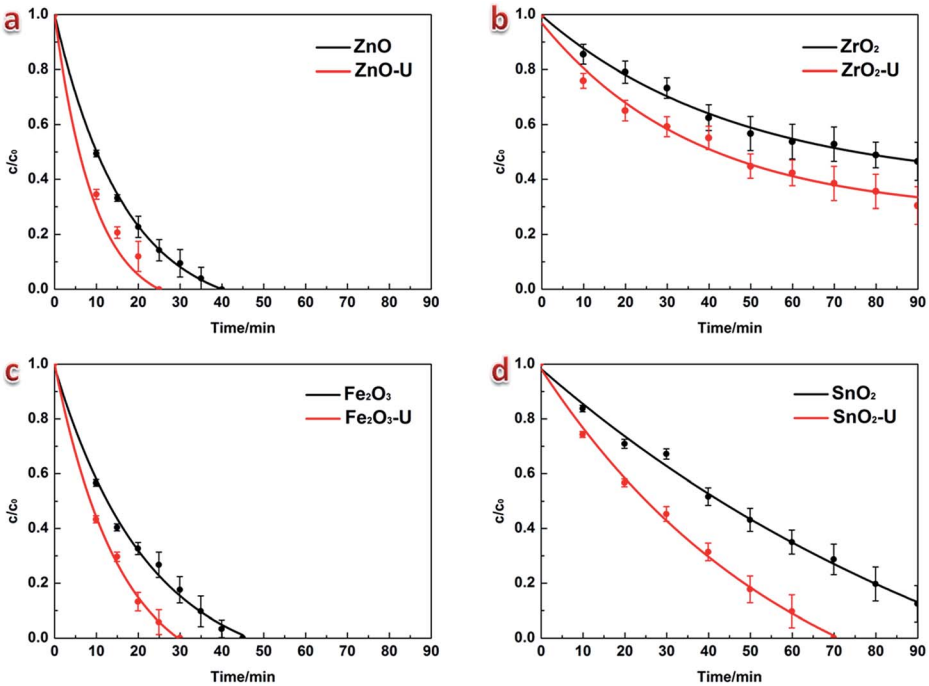

Fig. 5 Evaluations of solar-driven photocatalytic activity (AF degradation) of ZnO, ZrO_2, Fe_2O_3, SnO_2 NCs and the corresponding ultrasonic-treated products.

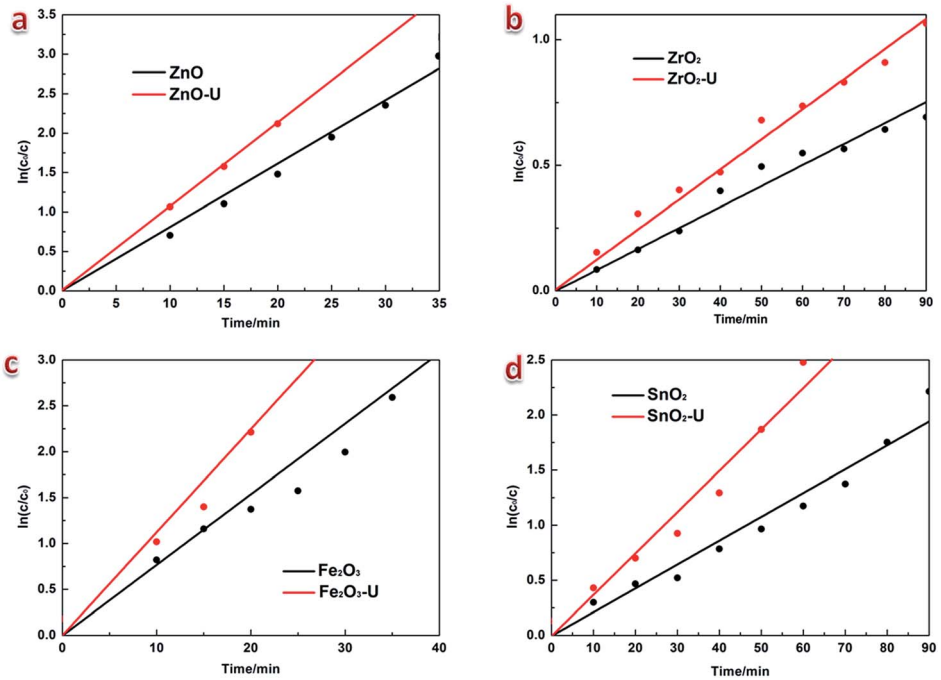

Fig. 6 Kinetic plots of solar-driven photocatalysis for ZnO, ZrO_2, Fe_2O_3, SnO_2 NCs and the corresponding ultrasonic-treated products.

energy is not high enough in visible-light,[44] but the enhanced light harvest induced by band gap narrowing could still make the better visible-light-driven photocatalytic performance. The experimental results confirm that visible-light-driven photocatalytic activity for AF degradation is increased for ~106% in ZnO NCs and ~239% in Fe_2O_3 NCs through ultrasonic irradiation (Fig. S7†). The characteristics of inhibited recombination of photo-generated charge carriers, narrowed band gap and increased surface area are all resulted from ultrasonic-induced disorder engineering, which indicates the critical role of it in the photocatalytic activity enhancement of ZnO, ZrO_2, Fe_2O_3 and SnO_2 NCs.

Conclusions

In summary, we have employed ultrasonic irradiation to modify the structure and properties of ZnO, ZrO_2, Fe_2O_3 and SnO_2 NCs. The physicochemical effects of ultrasonic irradiation facilitate the hydrolysis reaction and improve the hydroxyls injection of all these metal oxide semiconductor NCs, which leads to the disorder engineering around NCs. Such structure modification on these metal oxide semiconductor NCs changes their electronic structure with band tails and narrower band gaps, which further induces the wavelength-extended and intensity-enhanced optical absorption, resulting in the deeper colours in appearance. The lattice distortion and band gap narrowing that induced by disorder engineering are both important reasons for the better photocatalytic performance of ultrasonic-treated products, which give rise to characteristics including inhibited recombination of photo-generated charge carriers, more light energy harvest and increased surface area. The ultrasonic-induced disorder engineering is proved to be a universal and facile method to improve the optical properties of nanostructured ZnO, ZrO_2, Fe_2O_3 and SnO_2, which is also likely to apply to other metal oxide semiconductor NCs.

Acknowledgements

The authors gratefully acknowledge the financial support for this work from the National Natural Science Foundation of China (No. 51229201, 51272231).

Notes and references

1 L. E. Greene, *et al.*, *Nano Lett.*, 2005, **5**, 1231–1236.
2 A. Dev, S. K. Panda, S. Kar, S. Chakrabarti and S. Chaudhuri, *J. Phys. Chem. B*, 2006, **110**, 14266–14272.
3 N. Daneshvar, M. H. Rasoulifard, A. R. Khataee and F. Hosseinzadeh, *J. Hazard. Mater.*, 2006, **143**, 95–101.
4 J. J. Wu and C. H. Tseng, *Appl. Catal., B*, 2006, **66**, 51–57.
5 S. Xiao, L. Zhao and J. Lian, *Catal. Lett.*, 2014, **144**, 347–354.
6 M. J. Zhou, Y. Hu, Y. Liu, W. L. Yang and H. S. Qian, *CrystEngComm*, 2012, **14**, 7686–7693.
7 B. Shen, X. Zhang, H. Ma, Y. Yao and T. Liu, *J. Environ. Sci.*, 2013, **25**, 791–800.
8 Q. Xiang and J. Yu, *Chem. Soc. Rev.*, 2012, **41**, 782–796.
9 Y. K. Mi, *et al.*, *Catalysts*, 2013, **3**, 88–103.
10 M. Zelner, H. Minti, R. Reisfeld, H. Cohen and R. Tenne, *Chem. Mater.*, 1997, **9**, 2541–2543.
11 A. J. Cowan, *et al.*, *J. Am. Chem. Soc.*, 2011, **133**, 10134–10140.
12 G. Liu, *et al.*, *J. Mater. Chem.*, 2012, **22**, 9704–9713.
13 Z. H. Zhang, M. F. Hossain, T. Miyazaki and T. Takahashi, *Environ. Sci. Technol.*, 2010, **44**, 4741–4746.

14 C. Zhu, P. Wang, L. Wang, L. Han and S. Dong, *Nanoscale*, 2011, **3**, 4376–4382.
15 Y. Liu, Y. Jiao, B. Yin, S. Zhang, F. Qu and X. Wu, *Nano-Micro Lett.*, 2013, **5**, 234–241.
16 C. Yu, J. C. Yu, H. He and W. Zhou, *Rare Met.*, 2016, **35**, 211–222.
17 X. Liu, *et al.*, *Adv. Energy Mater.*, 2016, **6**, 1600452.
18 K. S. Suslick, *Science*, 1990, **247**, 1439–1445.
19 Y. Wang, *et al.*, *Adv. Mater.*, 2000, **12**, 1183–1186.
20 K. S. Suslick, S. B. Choe, A. A. Cichowlas and M. W. Grinstaff, *Nature*, 1991, **353**, 414–416.
21 M. C. Arenas, *et al.*, *Ultrason. Sonochem.*, 2013, **20**, 777–784.
22 J. C. Yu, J. Yu, W. Ho and L. Zhang, *Chem. Commun.*, 2001, **19**, 1942–1943.
23 J. Guo, *et al.*, *Ultrason. Sonochem.*, 2011, **18**, 1082–1090.
24 X. Liu, *et al.*, *Ultrason. Sonochem.*, 2011, **18**, 1043–1047.
25 H. He, *et al.*, *Chin. J. Catal.*, 2016, **37**, 1841–1850.
26 C. Yu, *et al.*, *J. Alloys Compd.*, 2011, **509**, 4547–4552.
27 C. Yu, W. Zhou and J. Yu, *Chin. J. Inorg. Chem.*, 2011, **27**, 2033–2038.
28 L. Zhang and J. C. Yu, *Chem. Commun.*, 2003, **16**, 2078–2079.
29 D. T. Nguyen and K. S. Kim, *Chem. Eng. J.*, 2015, **276**, 11–19.
30 Y. Cai, *et al.*, *Mater. Lett.*, 2013, **112**, 36–38.
31 Y. Cai, *et al.*, *CrystEngComm*, 2014, **16**, 6125–6140.
32 S. Ghosh, D. Majumder, A. Sen and S. Roy, *Mater. Lett.*, 2014, **130**, 215–217.
33 C. Yu, *et al.*, *J. Hazard. Mater.*, 2012, **237–238**, 38–45.
34 J. Wang, *et al.*, *Ultrason. Sonochem.*, 2009, **16**, 225–231.
35 J. Wang, *et al.*, *Ultrason. Sonochem.*, 2010, **17**, 642–648.
36 Y. Jiao, Y. Liu, F. Qu and X. Wu, *CrystEngComm*, 2014, **16**, 575–580.
37 C. Fan, *et al.*, *RSC Adv.*, 2016, **6**, 67444–67448.
38 C. Fan, *et al.*, *J. Alloys Compd.*, 2017, **703**, 96–102.
39 E. McCafferty and J. P. Wightman, *Surf. Interface Anal.*, 1998, **26**, 549–564.
40 Z. Zheng, *et al.*, *Chem. Commun.*, 2012, **48**, 5733–5735.
41 T. Xia and X. Chen, *J. Mater. Chem. A*, 2013, **1**, 2983–2989.
42 L. Shen, *et al.*, *J. Phys. Chem. C*, 2008, **112**, 8809–8818.
43 L. Liu, P. Y. Yu, X. Chen, S. S. Mao and D. Z. Shen, *Phys. Rev. Lett.*, 2013, **111**, 065505.
44 C. Chen, W. Ma and J. Zhao, *Chem. Soc. Rev.*, 2010, **39**, 4206–4219.

